Wide Field-of-View Vector Flow Imaging with Convex Array using Archimedean-Spiral Wavefronts

Kaya Takakusagi[1‡], Kei Mitsui[1], Riku Suzuki[1] Takuro Ishii[1,2] and Yoshifumi Saijo[1*]
([1]Grad. School of Biomed, Eng., Tohoku Univ.; [2]FRIS, Tohoku Univ.)

1. Introduction

Vector flow imaging (VFI) is a valuable modality particularly for assessing complex haemodynamics. One of the scenarios in demand is visualizing the blood flow property in the diseased abdominal aorta, such as the abdominal aortic aneurysms. This may be realized by a high frame-rate VFI technique with a convex array probe using vector Doppler methods using unfocused wavefronts steered at multiple angles.

Vector Doppler flow visualization with linear array probes using plane wave have been much reported, and a large angle span of multi-angle wavefronts can reduce errors and variability.[1)] In addition, sector probes have been used to image blood flow in the heart with vector Doppler approach using diverging waves, locating virtual sources, because plane waves are inappropriate in terms of field of view (FOV). However, the angle span of diverging wavefronts in FOV is too small.[2)]

Like sector probes, convex array probes are not suitable for emitting plane waves for imaging abdominal blood flow. This study aimed to propose a vector Doppler framework using unfocused wavefronts suited for convex array probes in order to realize VFI with wide FOV. In this paper, a dual-angle vector Doppler method using Archimedean-spiral wavefronts was implemented and the performances of different steering angles were evaluated.

2. Material and Methods

2.1 Vector Doppler method using Archimedean-spiral wavefronts

In the dual-angle vector Doppler method, a two-dimensional velocity vector $\boldsymbol{V}$ is estimated by the following equation,

$$\boldsymbol{AV} = 2\boldsymbol{v} \tag{1}$$

where $\boldsymbol{A}$, $\boldsymbol{V}$ and $\boldsymbol{v}$ are given by

$$\boldsymbol{V} = \begin{bmatrix} V_x \\ V_z \end{bmatrix}, \quad \boldsymbol{v} = \begin{bmatrix} v_1 \\ v_2 \end{bmatrix},$$
$$\boldsymbol{A} = \begin{bmatrix} \sin\varphi_{T1} + \sin\varphi_R & \cos\varphi_{T1} + \cos\varphi_R \\ \sin\varphi_{T2} + \sin\varphi_R & \cos\varphi_{T2} + \cos\varphi_R \end{bmatrix} \tag{2}$$

where v_1 and v_2 are two color Doppler velocities measured by transmitting beams in two different directions, φ_{T1} and φ_{T2} are the transmit angles of the two beams, and φ_R is the receive angle to the array.

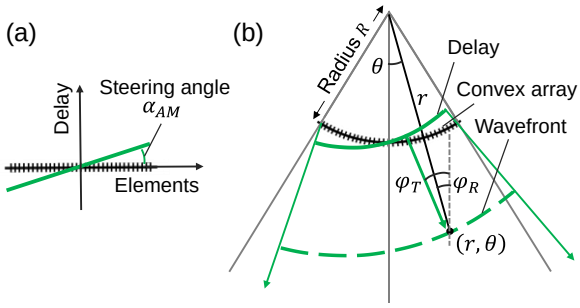

Fig. 1 (a) Linear transmit delay of steering angle α_{AMI}, (b) Archimedean-spiral wavefront, its transmit angle and receive angle.

Archimedean-spiral wavefronts is transmitted by giving a linear transmit delay tilted at steering angle α_{AM} to the convex array,[3)] as shown in **Fig. 1**. These wavefronts steered at several angles provide a wider overlapped region than that by simple steered plane waves, therefore allowing the wide FOV for the vector Doppler method. When transmitting two Archimedean-spiral wavefronts of steering angles $-\alpha_{AM}$ and $+\alpha_{AM}$ with convex probe, φ_{T1}, φ_{T2} and φ_R in eq. (2) is given by

$$\begin{cases} \varphi_{T1} = \arctan\left(\dfrac{R}{r}\tan(-\alpha_{AM})\right) + \theta \\ \varphi_{T2} = \arctan\left(\dfrac{R}{r}\tan(+\alpha_{AM})\right) + \theta \\ \varphi_R = \theta \end{cases} \tag{3}$$

where (r, θ) is the polar coordinates in Fig.1 and R is the radius of the convex array. Based on previous reports of vector Doppler method, the performance is expected to be largely dependent on φ_{T1}, φ_{T2} and the angle span $|\varphi_{T2} - \varphi_{T1}|$.

2.2 Experimental Setup

Phantom experiments were performed to evaluate the performance of the dual-angle vector Doppler method using the Archimedean-spiral wavefronts with different steering angles α_{AM}, that were 4, 8, 12, 16, 20 degrees in this study. A research-purpose ultrasound system (Vantage 256 system, Verasonics) equipped with a convex probe (128 elements, 0.48 mm pitch, 49.6 mm radius) was

‡kaya.takakusagi.s6@dc.tohoku.ac.jp, *saijo@tohoku.ac.jp

used to image a tilted straight flow channel of 5 mm in diameter (Doppler 403 flow phantom, Gammex).

Signal data were obtained by alternating emission of two Archimedean-spiral wavefronts of steering angles $\pm\alpha_{AM}$ with parameters of center frequency: 3.125 MHz, 3 cycle pulse, PRF: 2.3 kHz for each angle, and ensemble size: 32 for each angle. The signal data by two wavefronts were beamformed and processed respectively using a SVD clutter filtering and the lag-1 autocorrelator to obtain the color Doppler velocities v_1 and v_2. The velocity vector $\boldsymbol{V} = (V_x, V_z)$ was calculated by eq. (1)-(3).

Two different ROIs, P1 and P2, in the flow phantom were imaged and the flow at each position was visualized. P1 was from 40 to 60 mm in depth and from -10 to 10 mm in lateral distance (from the central axis of the probe), whereas P2 was at 15 mm deeper and 20 mm laterally farther away than the location of P1, which is harder to apply the simple vector Doppler method using steered plane waves. Velocity profiles vertical to the flow channel were sampled, and the temporal mean, temporal standard deviation (SD), and temporal mean absolute error (MAE) relative to a measured velocity were calculated for 20 consecutive frames. For this measured velocity, the absolute speed V_m was defined as the mean of V_{m1} and V_{m2}, which were the converted from color Doppler velocities v_1 and v_2, respectively. For example, V_{m1} was given by

$$V_{m1} = \frac{2v}{\cos(\varphi_{T1} - \theta_f) + \cos(\varphi_R - \theta_f)} \qquad (4)$$

where $\theta_f (= 52°)$ was the angle of the flow channel.

3. Results and discussion

Vector flow images and profiles by steering angle α_{AM} of 16 degrees are shown in **Fig. 2**. In both P1 and P2 ROIs, the estimated velocity vectors were mostly parallel to the flow channel, which showed the potential of Archimedean-spiral wavefronts for VFI with wide FOV. The temporal SD of both V_x and V_z in P2 were larger than those in P1.

The mean of the temporal SD and MAE on the estimated velocity profile of different steering angle α_{AM} are shown in **Fig. 3**. The mean SD and MAE were larger at P2, but they were smaller for larger α_{AM} in both P1 and P2. This leads to the expectation that a larger α_{AM} would provide smaller temporal variability and error of the estimation, regardless of the position.

The decrease in temporal SD and MAE might be directly caused by the increase of the transmit wavefront angle span $|\varphi_{T2} - \varphi_{T1}|$, which is larger for larger steering angle α_{AM} and smaller distance from origin r as shown in eq. (3).

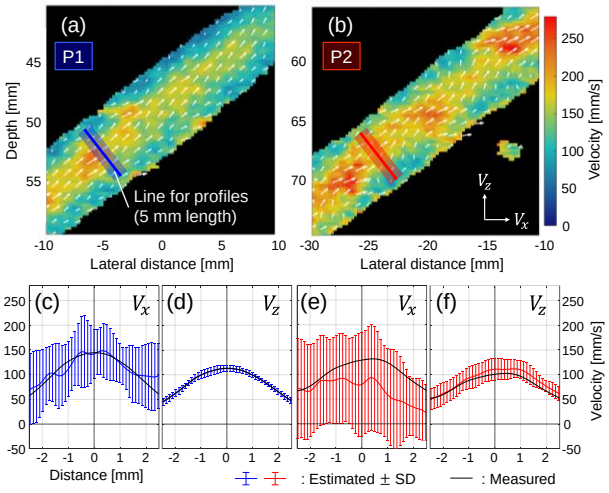

Fig. 2 (a) VFI in P1, (b) VFI in P2, (c) V_x profile in P1, (d) V_z profile in P1, (e) V_x profile in P2, (f) V_z in P2.

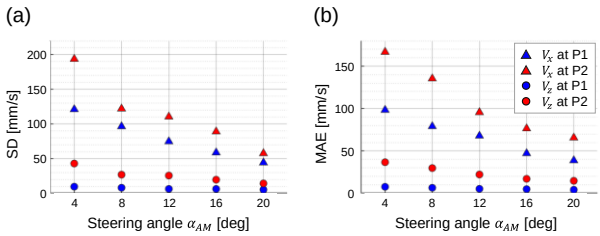

Fig. 3 (a) Mean of the temporal SD, (b) mean of the temporal MAE.

4. Conclusion

In this study, a VFI framework for a convex array probe using the Archimedean-spiral wavefronts was implemented and its performance with the different steering angles was evaluated.

The results showed the potential of Archimedean-spiral wavefronts for VFI with wide FOV. The larger steering angles were found to be superior in terms of the temporally variability and error, and thus the robust VFI could be achieved with the selection of appropriate steering angles. In the future, the effects of steering angle on accuracy and FOV need to be investigated further using phantom that mimics the abdominal aortic flow.

References

1) M. Maeda, R. Nagaoka, H. Ikeda, S. Yaegashi, and Y. Saijo, Jpn. J. Appl. Phys. **57,** 07LF02 (2018).
2) B. Y. Yiu, and A. C. Yu, IEEE Trans. Ultrason. Ferroelectr. Freq. Control **63**, 1733 (2016).
3) A. Besson, F. Wintzenrieth and C. Cohen-Bacrie, 2020 IEEE Int. Ultrason. Symp., 2020, p. 1.